HHS Public Access

Author manuscript

Adv Ther (Weinh). Author manuscript; available in PMC 2023 August 01.

Published in final edited form as:

Adv Ther (Weinh). 2022 August ; 5(8): . doi:10.1002/adtp.202200048.

Particle hydrogels decrease cerebral atrophy and attenuate astrocyte and microglia/macrophage reactivity after stroke

Elias Sideris[1], **Sophia Kioulaphides**[2], **Katrina Wilson**[2], **Aaron Yu**[1], **Jun Chen**[2], **S Thomas Carmichael**[3], **Tatiana Segura**[2,**]

[1]Department of Chemical and Biomolecular Engineering, University of California Los Angeles, Los Angeles, CA, United States

[2]Departments of Biomedical Engineering, Neurology, and Dermatology, Duke University, Durham, NC, United States

[3]Department of Neurology, David Geffen School of Medicine, University of California Los Angeles, Los Angeles, CA, United States

Abstract

Increasing numbers of individuals live with stroke related disabilities. Following stroke, highly reactive astrocytes and pro-inflammatory microglia can release cytokines and lead to a cytotoxic environment that causes further brain damage and prevents endogenous repair. Paradoxically, these same cells also activate pro-repair mechanisms that contribute to endogenous repair and brain plasticity. Here, we show that the direct injection of a hyaluronic acid based microporous annealed particle (MAP) hydrogel into the stroke core in mice reduces the percent of highly reactive astrocytes, increases the percent of alternatively activated microglia, decreases cerebral atrophy and preserves NF200 axonal bundles. Further, we show that MAP hydrogel promotes reparative astrocyte infiltration into the lesion, which directly coincides with axonal penetration into the lesion. This work shows that the injection of a porous scaffold into the stroke core can lead to clinically relevant decrease in cerebral atrophy and modulates astrocytes and microglia towards a pro-repair phenotype.

Graphical Abstract

**Corresponding author: Tel.: +1 919-660-2901, Tatiana.segura@duke.edu.

Author contributions: E.S., S.T.C., T.S. designed the experiments. E.S., A.Y., S.K., K.W., and J.C. performed experiments and analyzed data. E.S., S.T.C., T.S. wrote the manuscript with input from all authors.

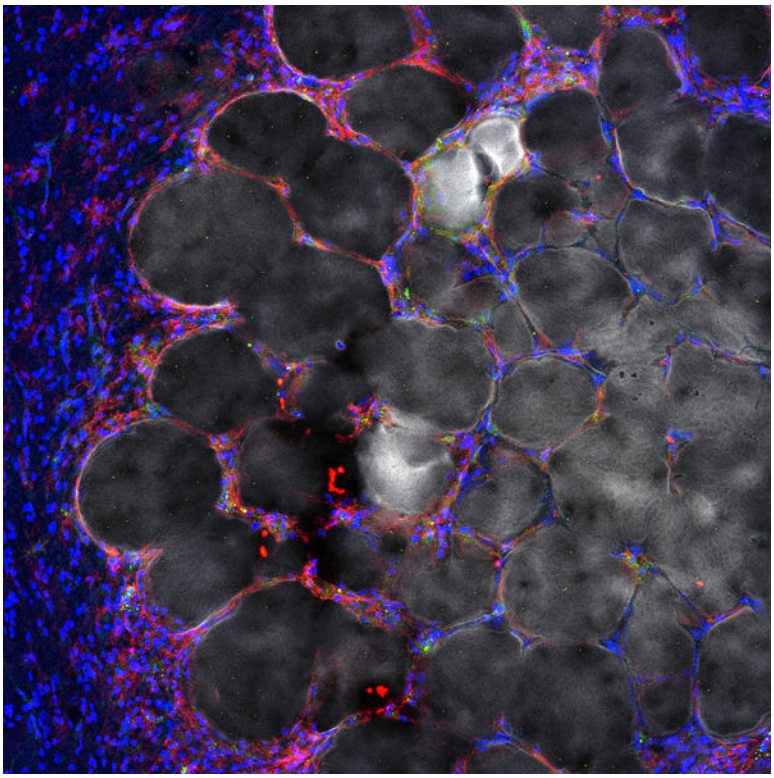

Injecting soft hyaluronic acid particle hydrogels into the stroke core prevents brain deformation, promotes astrocyte infiltration into the gel, and reduces the number of highly reactivity of astrocytes and microglia/macrophages that reside in the stroke core. Overall, particle hydrogel injection induces the formation of a pro-regenerative environment that results in axonal and progenitor cell infiltration.

Introduction

Stroke is the leading cause of adult long-term disability and affects 795,000 Americans every year [1]. Strokes occurs in two main forms, hemorrhagic or ischemic. Ischemic strokes are caused by an obstruction within a blood vessel, and account for 87% of all strokes and have a 32% mortality [2, 3]. For some stroke survivors the injury leaves them with a serious disability. There are currently no FDA approved therapies to treat long-term disability, leaving physical therapy as their only medical treatment.

Immediately following stroke onset, the lack of oxygen and nutrients causes significant cell death, a large influx of microglia/macrophages and the activation of highly reactive astrocytes, which release pro-inflammatory cytokines [4, 5], and lead to further neuronal death and a clearance of cellular debris [6]. Over time, the brain's defense mechanism is to compartmentalize the injured tissue from the surrounding tissue via an astrocytic border and fibrotic scar, with tissue fibrosis preventing repair in the stroke core [7]. With time, the stroke core is devoid of vessels and axons and cerebral atrophy occurs (brain shrinkage). Atrophy in the motor cortex accounts for at least a portion of the motor deficit in stroke patients

[8] and occurs at a rate of 0.95% of initial volume in the stroke hemisphere [9]. There are currently no therapies to prevent or treat cerebral atrophy, which is correlated with dementia [10], depression [11], and reduced motor function [8]

Astrocytes can both aid and obstruct stroke recovery [12, 13], with complete ablation of astrocytes resulting in a worse outcome after stroke[14]. Astrocytes are able to communicate with multiple neurons via secreted and contact-mediated signals, can coordinate the development of synapses [15–19] and neural circuits [20], yet astrocytes can limit long term repair and regeneration when a pro-inflammatory phenotype is adopted[12, 13]. Recently others [21–23] and we [24, 25] have published a number of publications injecting hydrogels into the stroke cavity. These studies have demonstrated that the stroke core can accept a significant gel injection volume without damage and that these gels can vary widely in composition ranging from hydrogels formed from decellularized native tissue [26], to peptide derived hydrogels [27], to synthetic hydrogels [28]. Although biomaterial strategies for brain repair have investigated astrocytes after stroke in the context of the glial scar, no biomaterial has been described that can modulate the astrocyte phenotype from inflammatory to pro-regenerative. Herein, we explore the use of hyaluronic acid based granular hydrogels to modulate astrocyte and microglia phenotype towards a pro-repair phenotype and the evaluation of the resulting reparative response.

Characterization of MAP hydrogel and stroke tissue

Microporous Annealed Particle (MAP) scaffolds are granular hydrogels generated from interlinked hydrogel microparticles (microgels). Hyaluronic acid (HA) microgels were generated using a previously described microfluidic flow focusing device [29] (Fig. 1A). HA (70–90 kDa) was utilized as our based material because it is a brain extracellular matrix component. Because microgels contained crosslinked hyaluronic acid, it behaves as high molecular weight, and thus is not expected to induce inflammation as has been reported for low molecular weight HA [30–32]. microgels used in this study were 80μm diameter (Fig. 1B,C) because we have previously found this diameter to be injectable and result in MAP scaffolds that were biocompatible in brain [24]. The Young's modulus of our MAP hydrogel is 927 Pa (Fig. 1D), which was chosen to match the Young's modulus of brain cortex [33]. Last, a key feature of MAP is interconnected void structure, which can be observed by filling the void space with fluorescently labeled dextran (Fig. 1E). Others and we have utilized MAP scaffolds for cell culture in vitro [24, 34–40] and support tissue ingrowth in vivo[24, 35–37]. In this study MAP scaffolds were injected into the stroke core at 5-days post wounding because a significant fluid filled cavity has been formed by this time that can accept a large volume of injection (Fig. 1F, G) [41]. MAP fills the stroke core as can be seen on the serial sections (Fig. 1H–K).

Injection of MAP hydrogel preserves long term structural integrity and function

To expand from our previous work using MAP scaffolds to treat stroke [24], we wanted to understand how long the gel lasts in the brain after implantation and if there are any detrimental effects of hydrogel injection long term. Our previous work focused only local tissue assessment at 2-weeks post stroke [24]. As previously done, we injected MAP hydrogel 5-days after stroke [41] and assessed for hydrogel degradation by monitoring hydrogel

fluorescence at days 2, 10, 30, 120 days post injection or 1, 2, 4, 16-weeks post stroke (Fig. 2A,B). We find that hydrogel fluorescence is visible at 4-weeks post stroke but not 16-weeks post stroke, indicating that the hydrogel can provide mechanical support for at least 30-days post injection.

Atrophy is commonly observed in stroke patients and is known to cause effects at regions far away from the stroke core [9]. In human patients' cerebral atrophy in the motor cortex accounts for at least a portion of the worsening motor deficit in stroke patients over time [8]. Thus, we wanted to get a sense if there are other visible effects of a long-lasting hydrogel in the brain post stroke and reduced cerebral atrophy in mice. We first wanted to understand if changes are to be expected due to ageing. Healthy mice that did not experience stroke or any other procedure were sacrificed at 1, 2, 4, 16-weeks (matching the age of the stroke mice). We find that in general, healthy mice brain size do not change with age and thus any changes in brain size in our experiments will be due to stroke related injury (Fig. 2C). We find that stroke (sham condition) induces statistically significant changes in brain volume and cortex volume that are reversed when MAP hydrogel is injected in the stroke core (Fig. 2C). We next wanted to compare the ratio of the ipsilateral (injured hemisphere) and contralateral (non-injured hemisphere), which directly address differences between the two hemispheres in the same animal. As with the global brain and cortex volume, healthy animals had no statistical difference between their two hemispheres, indicating their symmetry and that again any changes would be due to the stroke related injury and not age. We find that both stroke only (sham) and stroke + MAP injection (MAP) results in a statistical different ratio at 16-weeks. However, the change for the sham group is statistically significant at 4-weeks, but it is not for the MAP treated groups (Fig. 2D). Overall, we find that MAP gel injection delays significant changes in brain and cortex volume, which may have implications in delaying atrophy related disability.

We next wanted to assess how NF200 axonal bundles in the striatum vary across stroke only and MAP treated brains vary. These NF200 axonal bundles contain cortico-spinal, corticothalamic, cortico-bulbar and corticostriatal axonal projections. All of these are the major output of the cortex to subcortical sites and can be damaged after injury to the cortex and due to atrophy. We quantified the number of NF200 bundles over time using a watershed method to segment individual bundles. We report the ratio of number bundles between the two brain hemispheres. Although healthy animals have no statistical difference in NF200 axonal bundles in the striatum, they trend to a decrease with age. We find that at 4-weeks post stroke the stroke only condition (sham) has significantly reduced number of bundles compared to aged-match healthy controls and MAP treated brains suggesting that treatment with a hydrogel in the cortex can prevent damage to cortical axonal projections. Taken together the reduced cerebral atrophy and preservation of NF200 axonal bundles for MAP treated brains could reduce the long-term degenerative damage associated with these conditions.

Highly reactive, scar forming, astrocytes are reduced after MAP injection

We next moved to explore the use of MAP gels to modulate astrocyte phenotype. MAP gel was injected 5-days post stroke and tissue was collected 2-days post injection to assess the

early immune response to the material (Fig. 3A, B). We assessed both the peri-infarct (area surrounding the stroke core) for both stroke and stroke + MAP groups and the infarct area only for stroke + MAP because astrocytes do not infiltrate the stroke core in the absence of MAP injection. In the peri-infarct area, we observe a significantly higher percentage of reactive astrocytes in the sham condition expressing pERK1/2 (~56% compared to ~25% in MAP) (Fig. 3C), an astrocytic downstream pathway for high reactivity. Moreover, significantly fewer infiltrating astrocytes express pERK1/2 compared to those in the peri-infarct (~12% in the infarct compared to ~25% in the peri-infarct) (Fig. 3D). This data suggests that the astrocytes that are infiltrating the MAP gel are less reactive and potentially more pro-reparative. We also observe a significantly higher percentage of reactive astrocytes expressing S100β in the sham condition (~69%) compared to the 3.5% MAP gel (~26%), with high expression of S100β considered pathological[42, 43] (Fig. 3E). Like pERK expression, the infiltrating astrocytes expressing S100β (~15%) were significantly less than in the peri-infarct area (~26%). Additionally, we used *in situ* hybridization to dive deeper into the reactive astrocyte phenotype (Fig. 3F). Using RNA markers, we probed for C3, a marker shown to be upregulated in neurotoxic reactive astrocytes, and SLC1A2, a marker for all astrocytes [13]. Using a ratio of C3/SLC1A2 to analyze what percentage of astrocytes are highly reactive, we observed 54.2% of all astrocytes are reactive in the sham condition, while only 25.2% of all astrocytes are reactive in the 3.5% MAP gel peri-infarct condition. Comparing the peri-infarct of the MAP gel (~25.2%) to the infarct of the MAP gel (~10.7) once again further shows that the infiltrating astrocytes are less reactive and suggests a pro-regenerative phenotype (Fig. 3G). All these results indicate the MAP gel can attenuate astrocyte reactivity just two days after injection by reducing the number of highly reactive neurotoxic astrocytes by greater than 2-fold, promoting a less pro-inflammatory environment in the peri-infarct area and stimulating pro-recovery astrocyte infiltration in the infarct. Since inflammatory responses occur early after injury and initial inflammatory responses have long lasting effects in the tissue [4], we expect that early modulation of the astrogliotic response will have long lasting effects.

Microglia up-regulate pro-repair marker Arg1 in MAP

Microglial polarization directly affects astrocyte reactivity, with microglia that exhibit the more reactive M1 phenotype influencing astrocytes to a more highly reactive state [13]. Similar to the astrocyte experiments, MAP hydrogel was injected 5-days post stroke and tissue analyzed 2-days later (Fig. 3H). Though we recognize that microglia/macrophage exist in a spectrum of activation, we broadly defined pro-repair microglia/macrophages as expressing Arg1 and pro-inflammatory microglia/macrophages expressing iNOS [44]. Interestingly, the percentage of microglia/macrophages expressing the M1 pro-inflammatory phenotype is similar across both conditions in the peri-infarct and in the infarct (Fig. 3I). Further, the percentage of microglia/macrophages expressing the M2 pro-repair phenotype is similar across both conditions in the peri-infarct area. However, the percentage of pro-repair microglia/macrophages in the infarct, where the cells are encapsulated within HA-MAP during injection, is almost 3-fold higher in the MAP gel condition compared to sham condition (Fig. 3J). This suggests that the infarct in the MAP gel has a more pro-reparative environment than the infarct in the sham condition. Confinement of macrophages has been shown to prevent LPS polarized M1 macrophages to activate late-stage inflammatory genes

[45]. These findings combined with our findings of increased percentage of Arg1 positive cells, suggests that microporous hydrogels formed using ~80 μm microgels have pore sizes that can spatially confine the microglia and lower M1 polarization. Chondroitin sulfate proteoglycans (CSPGs) have been linked to decreased regenerative potential in the CNS [28, 46, 47]. We find that the amount of CSPGs in the HA-MAP treated mice significantly decreases in both the infarct (~5.3%) and peri-infarct (~9.8%) compared to sham infarct (~59.7%) and peri-infarct (~38%) (Supplemental Fig. 1). Several studies have delivered Chondroitinase ABC to digest the high release of CSPG after brain injury and shown behavioral functional benefits[46, 47]. Thus, a material such as HA-MAP that can decrease the CSPG level without additional enzyme delivery would be advantageous.

Astrocytes continue to infiltrate lesion over time:

One key difference between injection of MAP into the stroke cavity compared to any other hydrogel that we have tested [25, 48–51] is that it elicits astrocyte infiltration into the stroke cavity. Thus, rather than astrocytes remaining in the area surrounding the stroke core, as occurs in sham conditions, astrocytes change their morphology and begin to infiltrate. We observed this previously using a Middle Cerebral Artery occlusion (MCAo) model [24] and in data presented here with a PT stroke model, indicating the finding is not model or cortex location specific. To investigate if this change in morphology affects the scar thickness and if astrocyte infiltration is continuous over time, we injected HA-MAP 5-days after stroke and assessed scar thickness and astrocyte infiltration over time (7, 15, 30-days post stroke) by quantifying the thickness of the astrocyte (GFAP+) dense layer surrounding the stroke and infiltration distance of astrocytes starting from the stroke border (Fig. 4A, B). As expected, sham animals have scar thicknesses and peri-infarct % GFAP area that increases over time (7–30 days after stroke) (Fig. 4C), indicative of a developing scar [52]. In contrast, injection of MAP hydrogel into the stroke cavity significantly reduces the scar thickness and peri-infarct % GFAP area within 2-days of implantation and remains low throughout (Fig. 4D–F).

We next examined astrocyte (GFAP+) cell infiltration over time. We find that astrocyte infiltration begins within 2-days of hydrogel injection and continues to increase from 7–30-days post stroke, reaching close to 500μm into the lesion by day 30 (Fig. 4G). The infiltration pathway closely mimics what we expect is the void structure of the hydrogel (Fig. 1E), indicating that the cells infiltrate through the void space rather than through the microgels. This infiltration pattern further suggests that significant gel degradation is not required for astrocyte infiltration and that any degraded extracellular matrix (ECM) or new ECM deposition within the void space of HA-MAP does not prevent infiltration of astrocytes. We believe that promoting infiltration of pro-regenerative astrocytes into the infarct can be beneficial towards recovery [53]. This data also shows that the MAP gel sustains astrocyte infiltration over time without the need for biologic delivery such as growth factors or small molecules.

Microglia percent decreases over time for hydrogel injection:

Next, we examined microglia/macrophage reactivity over time using Iba1 staining (Fig. 4D). At two days post injection we find a 3-fold or 6-fold decrease in microglia stain for the peri-infarct (Fig. 4H) and infarct (Fig. 4I) area respectively when comparing sham to

HA-MAP treated strokes. As previously mentioned, reactive microglia have been shown to contribute to highly reactive astrocytes [13]. Further examination into microglial progression shows a very elevated total number of reactive microglia even 30 days post stroke (Fig. 4H, I). Remarkably, the total number of reactive microglia at 30 days post stroke in the infarct of the sham condition is still 3-fold higher than the infarct of the HA-MAP condition at 7 days post stroke, the peak of inflammation.

Astrocytes and axons co-infiltrate the stroke core after MAP injection:

Given the significant impact that MAP has on the phenotype of astrocytes and the number of microglia, we wanted to assess if changes in the stroke environment were accompanied with increases in axonogenesis. As before, HA-MAP hydrogel was injected into the stroke cavity 5-days after stroke and axonal area (NF200+) in the peri-infarct as well as infiltration distance in the infarct quantified (Fig. 5A, B). The peri-infarct percent NF200+ area decreases from 53.2% to 20.4% comparing un-injured brain and stroke brain at 5-days, indicating the rapid loss of neurofilaments in the peri-infarct space after stroke (Fig. 5C). The stroke cavity is devoid of neurofilaments at this timepoint. We find that axons (NF200+) increase in the peri-infarct space following injection of HA-MAP hydrogel, with a significant increase at 7-days post stroke compared with sham (Fig. 5D–F). However, this increase becomes non-significant at the 15- and 30-day timepoints. This data suggests that the lower number of reactive astrocytes combined with the decreased number in macrophage/microglia in the MAP condition, promotes a pro-reparative environment early after MAP injection that promotes axonal sprouting, but this environment cannot be maintained.

In the infarct cavity we observe axonal infiltration for the MAP hydrogel treated groups, but not in the sham groups. The path of infiltration is similar to what the astrocytes follow, navigating between the microgels rather than through the microgels (Fig. 5G). The infiltration distance of axons steadily increases over time reaching ~450μm by day 30 (Fig. 5G). Staining for both astrocytes (GFAP) and axons (NF200) revealed that not only do the axons follow the same path, but the axons appear to localize closely with the infiltrating astrocytes (Fig. 5H, I). High magnification image analysis revealed that although GFAP stain exists without axonal stain, the reverse is not true, whenever an axonal stain was present it was closely associated with GFAP staining. Examining the MAP hydrogel condition at 4-month reveals that the close association of axons and NF200 is maintained and that it is also accompanied by progenitor cells (SOX2+) (Fig. 5I). Although these images cannot determine the ratio of GFAP+, NF200+, and GFAP+/SOX2+ cells, we likely have all three cell types present within MAP hydrogel at 4 months post injection. Both recruitment of endogenous neural progenitor cells (NPCs) and transplantation of exogenous NPCs have been used as strategies to promote stroke repair and shown increase behavioral response[54]. This astrocyte/axon correlation suggests that the astrocytes are crucial for the axon penetration and maintenance, supporting our rationale that promotion of pro-repair astrocyte infiltration will be beneficial for downstream tissue repair. As prior studies have shown, these penetrating astrocytes, in very near proximity to axons could be crucial in forming synapses [15, 16, 19] and neuronal circuits directly in the lesion site [18, 20], where such recovery is not normally observed after stroke [4]. Although other molecules and cell types

maybe needed to generate the desired circuitry, having astrocytes, axons and NPCs in this same space can be now further manipulated to achieve this. Our results demonstrate that injection of MAP hydrogel into the stroke cavity is generating a permissible environment in the peri-infarct and infarct spaces that leads to axonal infiltration into the stroke core.

Vessel infiltration does not coincide with astrocyte/axonal infiltration:

Similar to axonal density, we observed an initial increase in vessel density (GLUT1 positive) in the peri-infarct space, which was statistically significant at the 15-day time-point compared to sham mice (Supplemental Fig. 2A-C). This result is consistent with other reports of stroke induced angiogenesis in the peri-infarct space [55]. However, by 30-days post stroke, there is no statistical significance in vessel density between MAP hydrogel injection and sham. Thus, like our axonal sprouting data, the increase in angiogenesis suggests that the lower microphage/microglia number and reduced reactive astrocytes in the peri-infarct space generates an environment that further promotes angiogenesis early after MAP gel injection, but that cannot be maintained long term.

After observing significant astrocyte/axonal infiltration into the stroke core, we tested if vessels also infiltrate the stroke core and if they follow a similar infiltration pattern (Supplemental Fig. 2D). We find that vessels infiltrate the stroke core, reaching a statistically significant difference of infiltrating vessels between brains treated with MAP and sham groups at 30-days post injection. The infiltration path is similar to that of astrocytes and axons, following the void space between microgels, but there appears to be no correlation between astrocyte infiltration and vessel infiltration, unlike what was observed for axonal infiltration. The vessel stain Glut-1 does not coincide with the astrocyte stain GFAP, indicating that vessels invade the stroke core independently. Further, we find that the vessel infiltration distance is significantly lower compared to what was found for astrocytes and axons (Supplemental Fig. 3). The average infiltration distance at 30-days for vessels is ~207μm while it is ~467μm for axons and astrocytes. This difference in infiltration distance is perplexing as HA-MAP hydrogel contains no releasable bioactive signals that would promote the infiltration of astrocytes and axons but not vessels. A few possibilities for the reduced infiltration distance for vessels are the physical properties of the gel, mechanical properties, and porosity. It is difficult to know what the mechanical properties of the gel are over time; however, the initial HA-MAP gel Young's modulus is ~1000Pa. It is possible that the mechanical modulus of the gel is not optimal for vessel infiltration, though others, including our lab, have used soft hydrogels for vascularization in the brain [35], skin [35], and bone [56]. Thus, mechanical properties are not likely to be the reason. The porosity of the scaffold is another possibility; HA-MAP gels with microgels of 80–100μm in diameter have a median pore area of ~200μm^2 which would correspond to 15–20μm when measured per z-stack [35, 57]. Although we have previously shown that PEG-MAP gels with 80μm diameter microgels promote vascularization and rapid wound closure in skin wounds [35], others have shown that in cardiac engineering there is limited vessel penetration in scaffolds with 20μm pores[58]. Thus, the effect in pore size in vascularization maybe tissue specific. Regardless of the reason, we have previously demonstrated that a robust vascular network within the stroke, promotes the formation of a neurovascular niche that leads to effective axonogenesis

and behavioral improvement [25]. Thus, efforts should be made to introduce pro-angiogenic cues into MAP to promote vascularization.

An additional rationale for further promoting vascularization is the fact that astrocytes and axons stopped infiltrating 200μm away from vessels, which is the oxygen diffusion limit [59]. Thus, lack of vascular infiltration, likely limited the range of astrocyte and axonal infiltration.

Moderate hydrogel stiffness changes do not affect astrocyte behavior:

Biomaterial and substrate stiffness has been previously shown to regulate astrocyte reactivity with softer substrates promoting astrocyte quiescence, suggesting that softer substrates should be used to better modulate astrocytes following stroke[60]. Stiffness has also been implicated in axonal sprouting, vessel sprouting and microglia polarization. We tested a moderately stiffer HA-MAP hydrogel (3.5% = 1000Pa, 4.5% = 1500Pa) to determine if this stiffness change can affect astrocyte behavior (Supplemental Fig. 4A, B). All other parameters, RGD concentration, microgel diameter, and void fraction were kept constant (Supplemental Fig. 4A, B). Overall, the 4.5% MAP hydrogel produced very similar results compared to the 3.5% hydrogel for astrocyte infiltration and scar thickness (Supplemental Fig. 4C, D). However, we did observe an increased number of reactive microglia in the infarct and in the peri-infarct at 2-weeks post stroke, but no significant differences were observed at 4-weeks post stroke (Supplemental Fig. 4E, F). Interestingly, these increased microglia response may have caused some downstream effects as we observe a slight decrease in axon penetration compared to the 3.5% condition (Supplemental Fig. 4G). It is possible that the increased number of microglia in the 4.5% condition created a more cytotoxic environment that affected the axon penetration.

Porosity, hyaluronic acid, and RGD are crucial for astrocyte infiltration:

We next wanted to examine if the observed responses are specific to the MAP formulation tested. MAP are produced from ~80μm microgels, which contain HA (70,000 Da, 3.5%), RGD (500μM), K and Q peptides (250μM), and 7.8mM of MMP crosslinker. The MAP gel is crosslinked using FXIIIa (5U/mL) and 1U/mL of thrombin. To test the role of microstructure on the observed findings, we compared the results from MAP to those of a hydrogel with identical composition but crosslinked as a bulk gel (non-porous) (Fig. 6A, B). As a comparison we tested the ability of these gels to promote astrocyte infiltration, reduce scar thickness and reduce the number of microphage/microglia in the peri-infarct and infarct spaces. We find that the scar thickness in the non-porous group is significantly reduced compared to sham but significantly larger compared to MAP (Fig. 6B). There is also no infiltration of astrocytes into the stroke cavity, suggesting that the microstructure of MAP is critical to this process. Microglia/macrophage area was significantly decreased in the infarct but not the peri-infarct compared to sham; however, the decrease was not as great as that observed with MAP.

We next tested the effect of the integrin binding ligand RGD. Injection of HA-MAP(-RGD) revealed that the scar thickness was again lower than sham, but not as low as HA-MAP. Similar to HA non-porous there was no infiltration of astrocytes into the stroke cavity,

pointing to the importance of RGD in this process. The number of reactive microglia for HA-MAP(-RGD) is similar to HA-MAP for the peri-infarct space, but significantly higher for infarct (Fig. 6C). Overall, we see that RGD has a major effect in the ability of HA-MAP to modulate astrocyte and microglia phenotype.

Last, we tested the role of the hydrogel backbone and compared HA to polyethylene glycol (PEG). PEG-vinyl sulfone (20,000Da) was used to generate microgels using the same concentration of K, Q and MMP peptides. PEG microgels were generated with RGD or no RGD. PEG microgels have the same diameter as HA microgels (Supplemental Fig. 4A) and the storage modulus is the same as HA-MAP (Supplemental Fig. 4B). We find that having a PEG backbone in the microgels significantly reduces the effect observed with HA-MAP. Scar thickness is significantly thinner than sham, but larger than HA-MAP and there is no significant difference between PEG-MAP and PEG-MAP(-RGD) (Fig. 6D). Astrocyte infiltration in the PEG-MAP or PEG-MAP(-RGD) conditions is also close to zero. Finally, the microphage/microglia area is significantly decreased in the infarct for both PEG-MAP or PEG-MAP(-RGD), but not statistically different from sham in the peri-infarct space. Overall, we find that HA is an essential component to promote infiltration of astrocytes into the infarct core.

Taken together this data shows that HA-MAP composition and microstructure is essential for the observed astrocyte infiltration, reduced scar thickness, and reduced microphage/microglia in the peri-infarct and infarct spaces. No other condition tested was equally effective as HA-MAP. Importantly, all the conditions that used HA as the backbone significantly decreased the scar thickness compared to conditions that used PEG as the backbone, demonstrating that the biological activity of HA plays an important role in this process. After stroke, CD44 expression is elevated in reactive astrocytes [61]. Thus, receptor mediated astrocyte/HA binding maybe responsible for the infiltration in HA-MAP but not PEG-MAP. Previous studies implanting porous HA-RGD hydrogels into cortex, demonstrated that RGD increased astrocyte infiltration into the cortex wound [62]. These results agree with our finding that HA-MAP but not HA-MAP(-RGD) promoted astrocyte infiltration. It is surprising that PEG-MAP and HA-MAP resulted in different tissue responses. These materials have the same microstructures and same concentration of RGD. Given the large number of studies conducted using PEG hydrogels for tissue repair applications, it is possible that the results observed here are particular to brain and not generalizable to all tissues. In our own laboratory, we have used PEG-MAP to treat skin wounds and shown substantial cellular infiltration and wound closure just 5-days after implantation [35].

Conclusions

Astrocytes have previously been thought to exacerbate the inflammation after stroke and be detrimental to recovery [5], however, recent studies show astrocytes with pro-regenerative phenotypes can be beneficial to the repair process[13]. When injected directly into the stroke cavity, MAP drastically affects the phenotype and reactivity state of the astrocytes just two days after injection. Using markers of highly reactive astrocytes, we show that the MAP hydrogel significantly reduces highly reactive astrocytic phenotype compared

to sham, while also promoting the infiltration of less reactive astrocytes into the lesion. Examination into microglial polarity suggested a more pro-repair environment compared to sham. Taken together, the MAP is able to modulate the brain's inflammatory response to the stroke by reducing highly reactive astrocytes and promoting infiltration of cells with a pro-reparative phenotype. The MAP hydrogel is able to sustain decreased inflammation over time by maintaining a reduced astrocytic scar, preventing a large influx of reactive microglia/macrophages, while extending astrocyte infiltration into the lesion. The ability of the MAP gel to modulate inflammation could transform treatments of severe inflammation in the brain. We hypothesize that spatial confinement and scaffold geometry are responsible for the observed changes. These effects of porous scaffolds have been observed in other tissues and in vitro assays [45, 63]. Further experimentation will be needed to elucidate the mechanism of MAP immune cell phenotype modulation.

By decreasing inflammation and promoting astrocytic infiltration, the MAP hydrogel is able to influence axonal penetration at the injured site. Every axon penetrating in the lesion is observed to be co-residing next to an infiltrating astrocyte. Meanwhile in the sham we observe minimal astrocyte and axon infiltration. This suggests that the less reactive astrocytes infiltrating into the lesion are partaking in the recovery process by supporting axonal infiltration. Thus, the anti-inflammatory effects of the HA-MAP hydrogel has downstream benefits by promoting increasing axonal penetration over time. Looking further downstream, we observe that the injection of the MAP hydrogel can provide mechanical support to the surrounding brain tissue by preventing the fibrotic pulling of the ventricle known as cerebral atrophy. With the combination of early on decreased inflammation and increased mechanical support provided by the MAP gel, the striatal pathway bundles, associated with motor function [64], are much better preserved compared to sham. This suggests that the ability of the MAP gel to modulate inflammation and support the tissue long term has significant downstream benefits and can lead to improved motor function.

Systematically testing effect of microstructure, RGD, and polymer backbone, we show that all three play crucial roles in modulating astrocyte infiltration. All injected hydrogels decreased inflammation to some extent, however, the MAP hydrogel significantly decreased the reactive microglial and astrocytic population the most. Moreover, only the MAP hydrogel was able to promote astrocyte infiltration into the lesion. This suggests that porosity and RGD are required for astrocyte infiltration, while receptor mediated astrocyte/HA binding could also be critical to infiltration.

The MAP hydrogel does have vascular limitations and further engineering is required of the material to improve the vascular response. Vascularization is critical to providing oxygen and nutrients to neighboring cells as its been shown that the oxygen diffusion limit is ~200μm. We observe the astrocytes and axons to be infiltrating ~200μm further than the infiltrating vessels. This suggests that the limiting factor to further astrocyte/axonal infiltration is the vessel response. Likely introducing delivery of angiogenic factors is required to improve the vasculature, infiltration and thereby, improving astrocyte/axonal infiltration.

Material and Methods

Microgel Production and Purification:

Microfluidic devices[35] and 3.5% microgels[65] were produced as previously described. Briefly, hyaluronic acid (HA) functionalized with an acrylate was dissolved at 7% (w/v) in 0.3M triethyloamine (TEOA) pH 8.8 and pre-reacted with K-peptide (Ac-FKGGERCG-NH_2) and Q-peptide (Ac-NQEQVSPLGGERCG-NH_2) at a final hydrogel concentration of 250μM, and RGD (Ac-RGDSPGERCG-NH_2) at a final hydrogel concentration of 500μM. Concurrently, the cross-linker solution was prepared by dissolving the di-thiol matrix metalloproteinase (MMP) sensitive peptide (Ac-GCRDGPQGIWGQDRCG-NH_2, Genscript) in distilled water at 7.8 mM and reacted with 10 μM Alexa-Fluor 647-maleimide (Life-Technologies) for 5 minutes. These solutions were mixed in a flow focusing microfluidic device and then immediately pinched by 1% span-80 in heavy mineral oil to form microspheres. These microspheres were collected and allowed to gel overnight at room temperature to form microgels. The microgels were then purified by repeated washes with HEPES buffer (pH 7.4 containing 10mM $CaCl_2$) and centrifugation. 4.5% microgels were produced in the same manner, however, the HA-acrylate precursor solution was dissolved at 9% (w/v). The HA without RGD microgels were produced with the same precursor solution as the 3.5% HA, however, no RGD was added. The PEG microgels were produced as previously described[35]. Briefly, 4-arm PEG-Vinyl sulfone (Jenkem) was dissolved at 10% (w/v) and the peptide concentrations were the same as the HA solutions.

Generation of Scaffold from Microgels and Mechanical Testing:

The microgels were pelleted by centrifuging at 18,000 G and the supernatant was discarded to form a concentrated solution of microgels. 5 U/mL of FXIII and 1 U/mL of Thrombin were combined in the presence of 10mM Ca^{2+} with the pelleted μgels and allowed to incubate at 37 °C for 90 minutes between two glass slides (1mm thickness) surface coated with sigmacote (Sigma-Aldrich). The mechanical testing on the hydrogel scaffolds was done using a 5500 series Instron. After annealing, the scaffolds were allowed to swell in HEPES buffer saline for 4 hours at room temperature. A 2.5N load cell with a 3.12mm tip in diameter was used at a compression strain rate of 1mm/min and the hydrogel scaffold was indented 0.8mm or 80% of its total thickness.

Nanoporous Hydrogel Production:

Nanoporous hydrogel precursor solutions were exactly the same as the microgel precursor solutions. Additionally, the same enzyme sensitive di-thiol cross-linker solution was prepared. These two solutions were thoroughly mixed in an Eppendorf tube by vortexing and pipetting. 5 U/mL of FXIII and 1 U/mL of Thrombin were added to the solution and the nanoporous hydrogel was allowed to gel *in situ* via the same Michael type addition in which the microgels were individually formed.

In Vivo Photothrombotic Stroke Model:

Animal procedures were performed in accordance with the US National Institutes of Health Animal Protection Guidelines, the University of California Los Angeles Chancellor's

Animal Research Committee, and Duke University Animal Research Committee (A016–21-01). A cortical photothrombotic stroke was induced on 8–12 week male C57BL/6 mice obtained from Jackson laboratories (Bar Harbor, ME). The mice were anesthetized with 2.5% isoflurane and placed onto a stereotactic setup. The mice were kept at 2.5% isoflurane in N2O:O2 for the duration of the surgery. A midline incision was made and Rose Bengal (10 mg/mL, Sigma-Aldrich) was injected intraperitoneally at 10 μL/g of mouse body weight. After 5 minutes of Rose Bengal injection, a 2-mm diameter cold fiberoptic light source was centered at 0 mm anterior/1.5 mm lateral left of the bregma for 18 minutes and a burr hole was drilled through the skull in the same location. All mice were given sulfamethoxazole and trimethoprim oral suspension (TMS, 303 mL TMS/250 mL H20, Amityville, NY) every 5 days for the entire length of the experiment. Five days following stroke surgery, microgels with FXIII were loaded into a Hamilton syringe (Hamilton Reno, NV) connected to a pump and 6 μL of microgels were injected into the stroke cavity using a 30-gauge needle at stereotaxic coordinates 0.26 mm anterior/posterior (AP), 3 mm medial/lateral (ML), and 1 mm dorsal/ventral (DV) with an infusion speed of 1μL/min. The needle was withdrawn from the mouse brain 5 minutes after the injection to allow for microgel annealing. For each condition a minimum of 5 mice was used.

1-, 2, 4, 16-weeks following stroke, mice were sacrificed via transcranial perfusion of 0.1 M PBS followed by 40 mL of 4 (w/v) % PFA. The brains were isolated and post-fixed in 4% PFA overnight and submerged in 30 (w/v) % sucrose solution for 24 hours. Tangential cortical sections of 30 μm-thickness were sliced using a cryostat and directly mounted on gelatin-subbed glass slides for immunobiological staining of GFAP (glial fibrillary acidic protein, Abcam, Cambridge, MA, USA) for astrocytes, IBA-1 (ionized calcium binding adaptor molecule, Abcam, Cambridge, MA, USA) for microglial cells, Glut-1 (Glucose Transporter-1, Abcam, Cambridge, MA, USA) for endothelial cells, NF200 (Neurofilament 200, Abcam, Cambridge, MA, USA) for axonal processes, pERK (Cell Signaling) for highly reactive astrocytes, S100β (thermofisher) for highly reactive astrocytes, CD11b (Abcam) for immune cells, Arginase 1 (Santa Cruz) for Pro-repair microglia/macrophages, NOS2 (Santa Cruz) for pro-inflammatory microglia/macrophages, Sox2 (Santa Cruz) for neural progenitor cells, and DAPI (1:500 Invitrogen) for nuclei. Primary antibodies (1:100) were incubated overnight at 4°C and secondary antibodies (1:1000) were incubated at room temperature for two hours. A Nikon C2 confocal microscope was used to take fluorescent images.

Image Analysis:

The IBA-1, GFAP, pERK, S100β, CD11b, Arg1, iNOS, CSPG, NF200, and Glut-1 astrocytic (GFAP) and positive area in the infarct and peri-infarct areas were quantified in 4 to 8 randomly chosen regions of interest (ROI of 0.3 mm^2) at a maximum distance of 300μm from the infarct for the peri-infarct and infarct analysis. In each ROI, the positive area was measured.

Ventricular Hypertrophy and Nigrostriatal Bundles Analysis (Figure 2):

Cryofrozen sections were allowed to thaw at room temperature. Sections were washed with PBS for 5 minutes with 3 repetitive washes. Sections were incubated with a 10% donkey serum and PBS with 0.3% triton at room temperature for one hour. The liquid was wicked

away and primary antibodies of GFAP (glial fibrillary acidic protein, Abcam, Cambridge, MA, USA) for astrocytes and NF200 (Neurofilament 200, Abcam, Cambridge, MA, USA) for axonal processes at 1:100 dilution in PBS with 0.3% triton and 10% donkey serum were added and incubated overnight at 4° C. The next day the primaries were washed with 3 repeated PBS washes of 5 minutes each. Secondary antibodies with donkey hosts along with Dapi at 1:1000 dilution in PBS with 0.3% triton and 10% donkey serum were added and incubated at room temperature for 2 hours. After two hours, the secondary antibodies were washed away with 3 repeated PBS washes of 5 minutes each. The sections were allowed to dry at room temperature and mounted using DPX mounting medium. Analyses were performed on microscope images of 3 coronal brain levels at +0.80 mm, −0.80 mm and −1.20 mm according to bregma, which consistently contained the cortical infarct area. Large scale 10x images of each section was taken and analyzed for ventricular hypertrophy. Cross-sectional areas in mm^2 were measured on FIJI and multiplied by 0.3 mm to calculate individual section volumes, and the 3 volumes of the ROI sections were added together to find the ROI volumes; each brain section was 0.03 mm thick, and there were 10 slides of brain sections per brain, thus one section was representative of 10 sections. Large scale 20x images were taken by the side of ventricle to analyze for nigrostriatal bundle area. Using pixel threshold on 8-bit converted images using ImageJ (Image J v1.43, Bethesda, Maryland, USA) and expressed as the area fraction of positive signal per area (%). Values were then averaged across all areas and sections, and expressed as the average positive area per animal. The number of NF200-stained bundles was analyzed in a ROI of 1 mm x 1 mm (Supplemental Fig. 5). These ROI were then converted into 8-bit images, then to binary images, were then watershed to split up bundles that may have merged, and then counted. Only bundles that were at least 400 μm^2 were counted.

Astrocyte Reactivity, IHC (Figure 3):

Cryofrozen sections were allowed to thaw at room temperature. Sections were washed with PBS for 5 minutes with 3 repetitive washes. Sections were incubated with a 10% donkey serum and PBS with 0.3% triton at room temperature for one hour. The liquid was wicked away and primary antibodies of GFAP (glial fibrillary acidic protein, Abcam, Cambridge, MA, USA) for astrocytes and pERK (Cell Signaling) for highly reactive astrocytes at 1:100 dilution in PBS with 0.3% triton and 10% donkey serum were added and incubated overnight at 4° C. The next day the primaries were washed with 3 repeated PBS washes of 5 minutes each. Secondary antibodies with donkey hosts along with Dapi at 1:1000 dilution in PBS with 0.3% triton and 10% donkey serum were added and incubated at room temperature for 2 hours. After two hours, the secondary antibodies were washed away with 3 repeated PBS washes of 5 minutes each. The sections were allowed to dry at room temperature and mounted using DPX mounting medium. Analyses were performed on microscope images of 3 coronal brain levels at +0.80 mm, −0.80 mm and −1.20 mm according to bregma, which consistently contained the cortical infarct area. Each image represents a maximum intensity projection of 10 to 12 Z-stacks, 1 μm apart, captured at a 20x magnification with a Nikon C2 confocal microscope using the NIS Element software. For the sham sections, using ImageJ and converting to 8-bit, a ratio of positive pERK area divided by positive GFAP area within the same area was taken to get percent of reactive astrocytes that are highly reactive in the peri-infarct area 0–300μm from the infarct border.

For the HA MAP sections, the peri-infarct were analyzed similarly to sham. The infarct was analyzed by taking 0–100μm infiltration into the lesion. S100β (thermofisher) was stained, imaged, and analyzed similarly to pERK.

Astrocyte Reactivity, HCR (Figure 3):

In situ hybridization probes for C3 and SLC1A2 were purchased from Molecular Instruments and the protocol published on the molecular instrument website was used to probe the sections. Analyses were performed on microscope images of 3 coronal brain levels at +0.80 mm, −0.80 mm and −1.20 mm according to bregma, which consistently contained the cortical infarct area. Large scale 40x images were taken using a Nikon C2 confocal along the stroke border. The images were than analyzed similar to pERK and S100β.

Microglial Reactivity (Figure 3):

Cryofrozen sections were allowed to thaw at room temperature. Sections were washed with PBS for 5 minutes with 3 repetitive washes. Sections were incubated with a 10% donkey serum and PBS with 0.3% triton at room temperature for one hour. The liquid was wicked away and primary antibodies of CD11b (Abcam) for immune cells, Arginase 1 (Santa Cruz) for Pro-repair microglia/macrophages, NOS2 (Santa Cruz) for pro-inflammatory microglia/macrophages at 1:100 dilution in PBS with 0.3% triton and 10% donkey serum were added and incubated overnight at 4° C. The next day the primaries were washed with 3 repeated PBS washes of 5 minutes each. Secondary antibodies with donkey hosts along with Dapi at 1:1000 dilution in PBS with 0.3% triton and 10% donkey serum were added and incubated at room temperature for 2 hours. After two hours, the secondary antibodies were washed away with 3 repeated PBS washes of 5 minutes each. The sections were allowed to dry at room temperature and mounted using DPX mounting medium. Analyses were performed on microscope images of 3 coronal brain levels at +0.80 mm, −0.80 mm and −1.20 mm according to bregma, which consistently contained the cortical infarct area. Each image represents a maximum intensity projection of 10 to 12 Z-stacks, 1 μm apart, captured at a 20x magnification with a Nikon C2 confocal microscope using the NIS Element software. In the peri-infarct for both sham and HA MAP, the ratio of the positive area of iNOS or Arg1 was divided by the positive area for CD11b from 0–300μm from the infarct border. In the infarct, the ratio of the positive area of iNOS or Arg1 was divided by the positive area for CD11b from 0–300μm from the infarct border.

Astrocyte and Microglial Progression Analysis (Figure 4):

Cryofrozen sections were allowed to thaw at room temperature. Sections were washed with PBS for 5 minutes with 3 repetitive washes. Sections were incubated with a 10% donkey serum and PBS with 0.3% triton at room temperature for one hour. The liquid was wicked away and primary antibodies of GFAP (glial fibrillary acidic protein, Abcam, Cambridge, MA, USA) for astrocytes, IBA-1 (ionized calcium binding adaptor molecule, Abcam, Cambridge, MA, USA) for reactive microglia/macrophages at 1:100 dilution in PBS with 0.3% triton and 10% donkey serum were added and incubated overnight at 4° C. The next day the primaries were washed with 3 repeated PBS washes of 5 minutes each. Secondary antibodies with donkey hosts along with Dapi at 1:1000 dilution in PBS with 0.3% triton and 10% donkey serum were added and incubated at room temperature

for 2 hours. After two hours, the secondary antibodies were washed away with 3 repeated PBS washes of 5 minutes each. The sections were allowed to dry at room temperature and mounted using DPX mounting medium. Analyses were performed on microscope images of 3 coronal brain levels at +0.80 mm, −0.80 mm and −1.20 mm according to bregma, which consistently contained the cortical infarct area. Each image represents a maximum intensity projection of 10 to 12 Z-stacks, 1 μm apart, captured at a 20x magnification with a Nikon C2 confocal microscope using the NIS Element software. Scar thickness was analyzed as distance from stroke border using astrocyte morphology changes to signify end of scar. Astrocyte infiltration was measured as longest infiltrating astrocyte from stroke border. In the peri-infarct for both sham and HA MAP, the percent positive for IBA-1 was measured 0–300μm from the infarct border. In the infarct, the percent positive for IBA-1 was measured 0–300μm from the infarct border.

Axon Progression (Figure 5):

Cryofrozen sections were allowed to thaw at room temperature. Sections were washed with PBS for 5 minutes with 3 repetitive washes. Sections were incubated with a 10% donkey serum and PBS with 0.3% triton at room temperature for one hour. The liquid was wicked away and primary antibodies of GFAP (glial fibrillary acidic protein, Abcam, Cambridge, MA, USA) for astrocytes and NF200 (Neurofilament 200, Abcam, Cambridge, MA, USA) for axonal processes at 1:100 dilution in PBS with 0.3% triton and 10% donkey serum were added and incubated overnight at 4° C. The next day the primaries were washed with 3 repeated PBS washes of 5 minutes each. Secondary antibodies with donkey hosts along with Dapi at 1:1000 dilution in PBS with 0.3% triton and 10% donkey serum were added and incubated at room temperature for 2 hours. After two hours, the secondary antibodies were washed away with 3 repeated PBS washes of 5 minutes each. The sections were allowed to dry at room temperature and mounted using DPX mounting medium. Analyses were performed on microscope images of 3 coronal brain levels at +0.80 mm, −0.80 mm and −1.20 mm according to bregma, which consistently contained the cortical infarct area. Each image represents a maximum intensity projection of 10 to 12 Z-stacks, 1 μm apart, captured at a 20x magnification with a Nikon C2 confocal microscope using the NIS Element software. Axon infiltration was measured as longest infiltrating neurofilament from stroke border. In the peri-infarct for both sham and HA MAP, the percent positive for NF200 was measured 0–300μm from the infarct border. In the infarct, the percent positive for NF200 was measured 0–300μm from the infarct border.

Vessel Progression (Supplemental Figure):

Cryofrozen sections were allowed to thaw at room temperature. Sections were washed with PBS for 5 minutes with 3 repetitive washes. Sections were incubated with a 10% donkey serum and PBS with 0.3% triton at room temperature for one hour. The liquid was wicked away and primary antibodies of GFAP (glial fibrillary acidic protein, Abcam, Cambridge, MA, USA) for astrocytes and Glut-1 (Glucose Transporter-1, Abcam, Cambridge, MA, USA) for endothelial cells at 1:100 dilution in PBS with 0.3% triton and 10% donkey serum were added and incubated overnight at 4° C. The next day the primaries were washed with 3 repeated PBS washes of 5 minutes each. Secondary antibodies with donkey hosts along with Dapi at 1:1000 dilution in PBS with 0.3% triton and 10% donkey serum were added

and incubated at room temperature for 2 hours. After two hours, the secondary antibodies were washed away with 3 repeated PBS washes of 5 minutes each. The sections were allowed to dry at room temperature and mounted using DPX mounting medium. Analyses were performed on microscope images of 3 coronal brain levels at +0.80 mm, −0.80 mm and −1.20 mm according to bregma, which consistently contained the cortical infarct area. Each image represents a maximum intensity projection of 10 to 12 Z-stacks, 1 μm apart, captured at a 20x magnification with a Nikon C2 confocal microscope using the NIS Element software. Vessel infiltration was measured as longest infiltrating vessel from stroke border. In the peri-infarct for both sham and HA MAP, the percent positive for Glut1 was measured 0–300μm from the infarct border. In the infarct, the percent positive for Glut1 was measured 0–300μm from the infarct border.

Statistical Analysis:

Minimum animal group sample size was determined to be 5 by using a statistical power analysis that compares the mean value and standard deviation of a selected experiment (microglia surface % in the peri-infarct area 2 weeks after stroke) in a selected animal condition (HA-MAP) performed in a pilot study compared with a previously published finding on the same experiment, condition, and time point (Lam, J et al, Adv Funct Mater 2014). The alpha value (Type 1 error) was fixed at the level of 5% ($P = 0.05$) and the power at 80%. There was no preprocessing of the data to remove outliers. Some analyses involve comparing the injured (ipsilateral) and non-injured (contralateral) brain regions. In these cases, quantification of the ipsilateral region was divided by the contralateral region. A value of 1 would indicate no difference between the injured and non-injured regions. In plots comparing groups for a particular day, standard box plots are used, which display the minimum and maximum value, the median quartile 1, quartile 3 and each individual values. Plots that show trends over time are plotted as the mean with standard deviation. Significance was analyzed using alpha = 0.05 and $p < 0.05$ was considered significant. One-way ANOVA, two-way ANOVA and t-test were used as detailed in the figure legends. GraphPad Prism 9 for MacOS was used for all statistical analyses.

Supplementary Material

Refer to Web version on PubMed Central for supplementary material.

Acknowledgements:

The authors would like to acknowledge Dr. Amy Gleichman for her expertise on astrocytes and helpful discussion. The authors would like thank Dr. Irene Llorente for her help on quantification methods. The authors would like to acknowledge Dr. Lina Nih for her assistance with tissue collection and helpful discussions. The authors would like thank Katrina Wilson for her help producing microgels. The authors would like to thank the entire Carmichael lab at UCLA for their stroke expertise and help. We would like to acknowledge the National Institutes of Health and the National Institute for Neurological Diseases and Stroke for funding (R01NS094599, 1R01NS112940, 1R01NS079691).

References

1. Benjamin EJ et al. Heart Disease and Stroke Statistics-2017 Update: A Report From the American Heart Association. Circulation 135, e146–e603 (2017). [PubMed: 28122885]

2. Foulkes MA, Wolf PA, Price TR, Mohr JP & Hier DB The Stroke Data Bank: design, methods, and baseline characteristics. Stroke 19, 547–554 (1988). [PubMed: 3363586]

3. Lloyd-Jones D et al. Heart disease and stroke statistics−−2009 update: a report from the American Heart Association Statistics Committee and Stroke Statistics Subcommittee. Circulation 119, 480–486 (2009). [PubMed: 19171871]

4. Carmichael ST The 3 Rs of Stroke Biology: Radial, Relayed, and Regenerative. Neurotherapeutics 13, 348–359 (2016). [PubMed: 26602550]

5. Dirnagl U, Iadecola C & Moskowitz MA Pathobiology of ischaemic stroke: an integrated view. Trends Neurosci 22, 391–397 (1999). [PubMed: 10441299]

6. Morales I, Guzman-Martinez L, Cerda-Troncoso C, Farias GA & Maccioni RB Neuroinflammation in the pathogenesis of Alzheimer's disease. A rational framework for the search of novel therapeutic approaches. Front Cell Neurosci 8, 112 (2014). [PubMed: 24795567]

7. Sofroniew MV & Vinters HV Astrocytes: biology and pathology. Acta Neuropathol 119, 7–35 (2010). [PubMed: 20012068]

8. Gauthier LV, Taub E, Mark VW, Barghi A & Uswatte G Atrophy of spared gray matter tissue predicts poorer motor recovery and rehabilitation response in chronic stroke. Stroke 43, 453–457 (2012). [PubMed: 22096036]

9. Seghier ML, Ramsden S, Lim L, Leff AP & Price CJ Gradual lesion expansion and brain shrinkage years after stroke. Stroke 45, 877–879 (2014). [PubMed: 24425126]

10. Neary D et al. Cerebral biopsy in the investigation of presenile dementia due to cerebral atrophy. J Neurol Neurosurg Psychiatry 49, 157–162 (1986). [PubMed: 3950634]

11. Sheline YI Hippocampal atrophy in major depression: a result of depression-induced neurotoxicity? Mol Psychiatry 1, 298–299 (1996). [PubMed: 9118352]

12. Gleichman AJ & Carmichael ST Astrocytic therapies for neuronal repair in stroke. Neurosci Lett 565, 47–52 (2014). [PubMed: 24184876]

13. Liddelow SA et al. Neurotoxic reactive astrocytes are induced by activated microglia. Nature 541, 481–487 (2017). [PubMed: 28099414]

14. Hayakawa K et al. Inhibition of reactive astrocytes with fluorocitrate retards neurovascular remodeling and recovery after focal cerebral ischemia in mice. J Cereb Blood Flow Metab 30, 871–882 (2010). [PubMed: 19997116]

15. Allen NJ et al. Astrocyte glypicans 4 and 6 promote formation of excitatory synapses via GluA1 AMPA receptors. Nature 486, 410–414 (2012). [PubMed: 22722203]

16. Christopherson KS et al. Thrombospondins are astrocyte-secreted proteins that promote CNS synaptogenesis. Cell 120, 421–433 (2005). [PubMed: 15707899]

17. Kucukdereli H et al. Control of excitatory CNS synaptogenesis by astrocyte-secreted proteins Hevin and SPARC. Proc Natl Acad Sci U S A 108, E440–449 (2011). [PubMed: 21788491]

18. Pascual O et al. Astrocytic purinergic signaling coordinates synaptic networks. Science 310, 113–116 (2005). [PubMed: 16210541]

19. Stellwagen D & Malenka RC Synaptic scaling mediated by glial TNF-alpha. Nature 440, 1054–1059 (2006). [PubMed: 16547515]

20. Clarke LE & Barres BA Emerging roles of astrocytes in neural circuit development. Nat Rev Neurosci 14, 311–321 (2013). [PubMed: 23595014]

21. Massensini AR et al. Concentration-dependent rheological properties of ECM hydrogel for intracerebral delivery to a stroke cavity. Acta Biomater 27, 116–130 (2015). [PubMed: 26318805]

22. Gorenkova N, Osama I, Seib FP & Carswell HV In vivo evaluation of engineered self-assembling silk fibroin hydrogels after intracerebral injection in a rat stroke model. ACS Biomaterials Science & Engineering 5, 859–869 (2018). [PubMed: 33405845]

23. Payne SL et al. Initial cell maturity changes following transplantation in a hyaluronan-based hydrogel and impacts therapeutic success in the stroke-injured rodent brain. Biomaterials 192, 309–322 (2019). [PubMed: 30468998]

24. Nih LR, Sideris E, Carmichael ST & Segura T Injection of Microporous Annealing Particle (MAP) Hydrogels in the Stroke Cavity Reduces Gliosis and Inflammation and Promotes NPC Migration to the Lesion. Adv Mater 29 (2017).

25. Nih LR, Gojgini S, Carmichael ST & Segura T Dual-function injectable angiogenic biomaterial for the repair of brain tissue following stroke. Nat Mater 17, 642–651 (2018). [PubMed: 29784996]
26. Saldin LT, Cramer MC, Velankar SS, White LJ & Badylak SF Extracellular matrix hydrogels from decellularized tissues: Structure and function. Acta Biomater 49, 1–15 (2017). [PubMed: 27915024]
27. Hong A et al. Self-assembling injectable peptide hydrogels for emerging treatments of ischemic stroke. Journal of Materials Chemistry B (2019).
28. Hettiaratchi MH et al. Local delivery of stabilized chondroitinase abc degrades chondroitin sulfate proteoglycans in stroke-injured rat brains. Journal of controlled release 297, 14–25 (2019). [PubMed: 30690102]
29. Sideris E et al. Particle Hydrogels Based on Hyaluronic Acid Building Blocks. Acs Biomater Sci Eng 2, 2034–2041 (2016). [PubMed: 33440539]
30. Zhao Y et al. A novel neuroinflammation-responsive hydrogel based on mimicking naked mole rat brain microenvironment retards neurovascular dysfunction and cognitive decline in Alzheimer's disease. Chemical Engineering Journal 430, 133090 (2022).
31. Petrey AC & de la Motte CA Hyaluronan, a crucial regulator of inflammation. Front Immunol 5, 101 (2014). [PubMed: 24653726]
32. Tavianatou AG et al. Hyaluronan: molecular size-dependent signaling and biological functions in inflammation and cancer. FEBS J 286, 2883–2908 (2019). [PubMed: 30724463]
33. Budday S et al. Mechanical properties of gray and white matter brain tissue by indentation. J Mech Behav Biomed Mater 46, 318–330 (2015). [PubMed: 25819199]
34. Caldwell AS, Campbell GT, Shekiro KMT & Anseth KS Clickable Microgel Scaffolds as Platforms for 3D Cell Encapsulation. Adv Healthc Mater 6 (2017).
35. Griffin DR, Weaver WM, Scumpia PO, Di Carlo D & Segura T Accelerated wound healing by injectable microporous gel scaffolds assembled from annealed building blocks. Nat Mater 14, 737–744 (2015). [PubMed: 26030305]
36. Hsu R-S et al. Adaptable Microporous Hydrogels of Propagating NGF-Gradient by Injectable Building Blocks for Accelerated Axonal Outgrowth. Advanced Science 0, 1900520.
37. Mealy JE et al. Injectable Granular Hydrogels with Multifunctional Properties for Biomedical Applications. Adv Mater 30, e1705912 (2018). [PubMed: 29602270]
38. Truong NF, Lesher-Perez SC, Kurt E & Segura T Pathways Governing Polyethylenimine Polyplex Transfection in Microporous Annealed Particle Scaffolds. Bioconjug Chem 30, 476–486 (2019). [PubMed: 30513197]
39. Xin S, Chimene D, Garza JE, Gaharwar AK & Alge DL Clickable PEG hydrogel microspheres as building blocks for 3D bioprinting. Biomaterials science (2019).
40. Xin S, Wyman OM & Alge DL Assembly of PEG Microgels into Porous Cell-Instructive 3D Scaffolds via Thiol-Ene Click Chemistry. Adv Healthc Mater 7, e1800160 (2018). [PubMed: 29663702]
41. Wilson KL, Carmichael ST & Segura T Injection of Hydrogel Biomaterial Scaffolds to The Brain After Stroke. J Vis Exp (2020).
42. Mori T et al. Overexpression of human S100B exacerbates cerebral amyloidosis and gliosis in the Tg2576 mouse model of Alzheimer's disease. Glia 58, 300–314 (2010). [PubMed: 19705461]
43. Michetti F et al. The S100B story: from biomarker to active factor in neural injury. J Neurochem 148, 168–187 (2019). [PubMed: 30144068]
44. Miron VE et al. M2 microglia and macrophages drive oligodendrocyte differentiation during CNS remyelination. Nat Neurosci 16, 1211–1218 (2013). [PubMed: 23872599]
45. Jain N & Vogel V Spatial confinement downsizes the inflammatory response of macrophages. Nat Mater 17, 1134–1144 (2018). [PubMed: 30349032]
46. Moon LD, Asher RA, Rhodes KE & Fawcett JW Regeneration of CNS axons back to their target following treatment of adult rat brain with chondroitinase ABC. Nat Neurosci 4, 465–466 (2001). [PubMed: 11319553]
47. Bradbury EJ et al. Chondroitinase ABC promotes functional recovery after spinal cord injury. Nature 416, 636–640 (2002). [PubMed: 11948352]

48. Lam J, Lowry WE, Carmichael ST & Segura T Delivery of iPS-NPCs to the Stroke Cavity within a Hyaluronic Acid Matrix Promotes the Differentiation of Transplanted Cells. Adv Funct Mater 24, 7053–7062 (2014). [PubMed: 26213530]
49. Nih LR et al. Engineered HA hydrogel for stem cell transplantation in the brain: Biocompatibility data using a design of experiment approach. Data Brief 10, 202–209 (2017). [PubMed: 27995155]
50. Moshayedi P et al. Systematic optimization of an engineered hydrogel allows for selective control of human neural stem cell survival and differentiation after transplantation in the stroke brain. Biomaterials 105, 145–155 (2016). [PubMed: 27521617]
51. Li S et al. Hydrogels with precisely controlled integrin activation dictate vascular patterning and permeability. Nat Mater 16, 953–961 (2017). [PubMed: 28783156]
52. Badan I et al. Accelerated glial reactivity to stroke in aged rats correlates with reduced functional recovery. J Cereb Blood Flow Metab 23, 845–854 (2003). [PubMed: 12843788]
53. Weber B & Barros LF The Astrocyte: Powerhouse and Recycling Center. Cold Spring Harb Perspect Biol 7 (2015).
54. Carmichael ST Emergent properties of neural repair: elemental biology to therapeutic concepts. Ann Neurol 79, 895–906 (2016). [PubMed: 27043816]
55. Ohab JJ, Fleming S, Blesch A & Carmichael ST A neurovascular niche for neurogenesis after stroke. J Neurosci 26, 13007–13016 (2006). [PubMed: 17167090]
56. Giavaresi G et al. Blood vessel formation after soft-tissue implantation of hyaluronan-based hydrogel supplemented with copper ions. Biomaterials 26, 3001–3008 (2005). [PubMed: 15603795]
57. Sideris E et al. Particle hydrogels based on hyaluronic acid building blocks. ACS Biomaterials Science & Engineering 2, 2034–2041 (2016). [PubMed: 33440539]
58. Madden LR et al. Proangiogenic scaffolds as functional templates for cardiac tissue engineering. Proc Natl Acad Sci U S A 107, 15211–15216 (2010). [PubMed: 20696917]
59. Carmeliet P & Jain RK Angiogenesis in cancer and other diseases. Nature 407, 249–257 (2000). [PubMed: 11001068]
60. Wilson CL, Hayward SL & Kidambi S Astrogliosis in a dish: Substrate stiffness induces astrogliosis in primary rat astrocytes. RSC Advances 6, 34447–34457 (2016). [PubMed: 32742641]
61. Konopka A et al. Cleavage of Hyaluronan and CD44 Adhesion Molecule Regulate Astrocyte Morphology via Rac1 Signalling. PLoS One 11, e0155053 (2016). [PubMed: 27163367]
62. Cui FZ, Tian WM, Hou SP, Xu QY & Lee IS Hyaluronic acid hydrogel immobilized with RGD peptides for brain tissue engineering. J Mater Sci Mater Med 17, 1393–1401 (2006). [PubMed: 17143772]
63. Brown BN, Ratner BD, Goodman SB, Amar S & Badylak SF Macrophage polarization: an opportunity for improved outcomes in biomaterials and regenerative medicine. Biomaterials 33, 3792–3802 (2012). [PubMed: 22386919]
64. Schallert T et al. Tactile extinction: distinguishing between sensorimotor and motor asymmetries in rats with unilateral nigrostriatal damage. Pharmacol Biochem Behav 16, 455–462 (1982). [PubMed: 7079281]
65. Sideris E et al. Particle hydrogels based on hyaluronic acid building blocks. ACS Biomaterials Science & Engineering (2016).

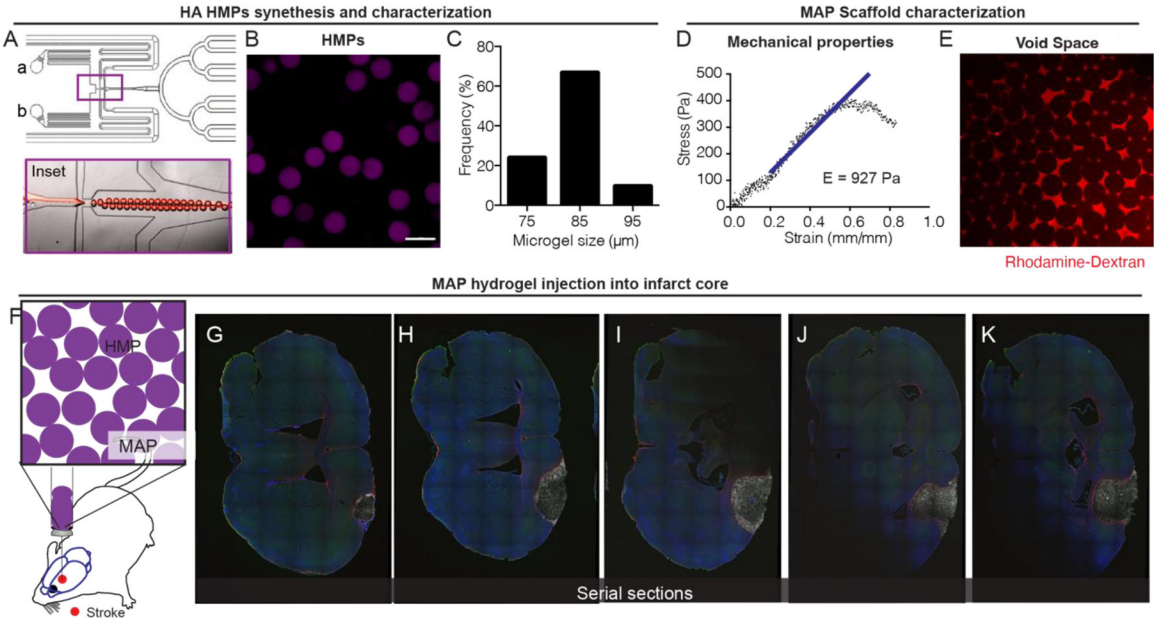

Figure 1.

A. flow-focusing microfluidic device used to produce hydrogel microparticles (microgels) via a water-in-oil emulsion. Inset shows flow focusing region. B. Image of microgels in aqueous solution. Scale bar = 100μm C. Histogram of microgel diameter. D. Instron mechanical compression testing of MAP scaffold after annealing of microgels. E. Image of high molecular weight fluorescent dextran between the MAP void spaces showing interconnected porosity. F. Injection schematic showing direct injection into the stroke cavity. G-K. Images of serial sections of a single stroked brain treated with MAP with each progressive section ~300μm apart.

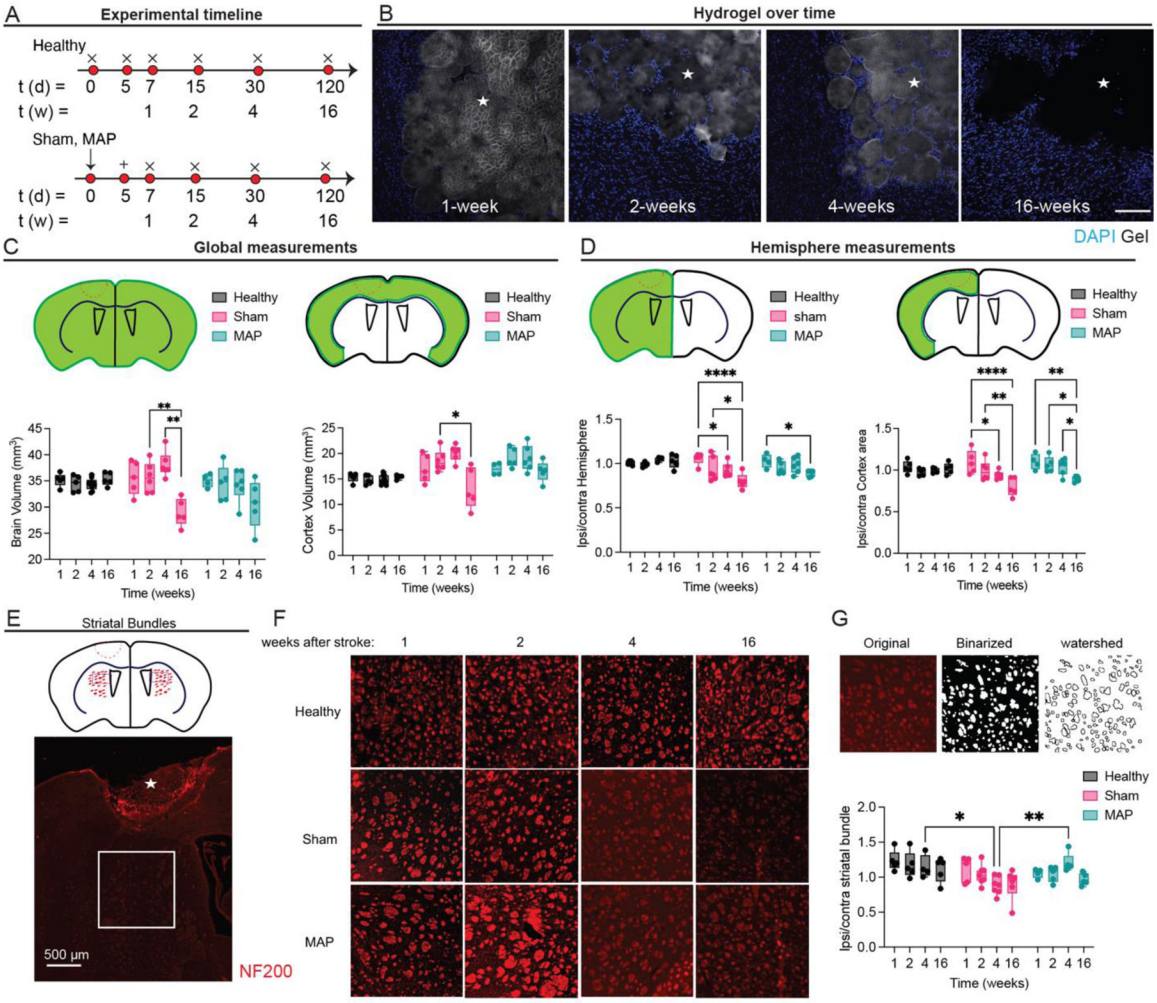

Figure 2.

A. Schematic of experimental timeline where arrow signifies stroke day, + signifies injection day (MAP only), and x signifies sacrifice and analysis time point. Sham is stroke only with no injection. B. Hydrogel imaging over time after stroke (1-, 2-, 4-, 16 weeks post stroke). Scale bar = 100 μm. C. Global measurements of brain and cortex volume for healthy, sham and MAP treated groups. D. Ratios of hemisphere and cortex area comparing ipsilateral to contralateral regions for healthy (no injury), sham (stroke only) and MAP (stroke + MAP) treated groups. E. Schematic of NF200 axonal bundles in hemispheres ipsilateral and contralateral to the lesion, showing ROI presented in F. F. NF200 axonal bundles over time for healthy, sham and MAP. G. shows ipsilateral to contralateral ratios of NF200 axonal bundles number for healthy, sham and MAP treated groups. All measurements were done on FIJI. Statistical analysis was done in GraphPad Prism using two-way ANOVA analysis of variance followed by a multiple comparisons test comparing each condition across time or between condition at each timepoint. The dots in each plot indicate the number of animals (n = 5 biological replicates) that were analyzed per-group and were considered independent experiments. *, **, ***, **** means $p < 0.05$, 0.01, 0.001, 0.0001. ☆ represents the stroke cavity.

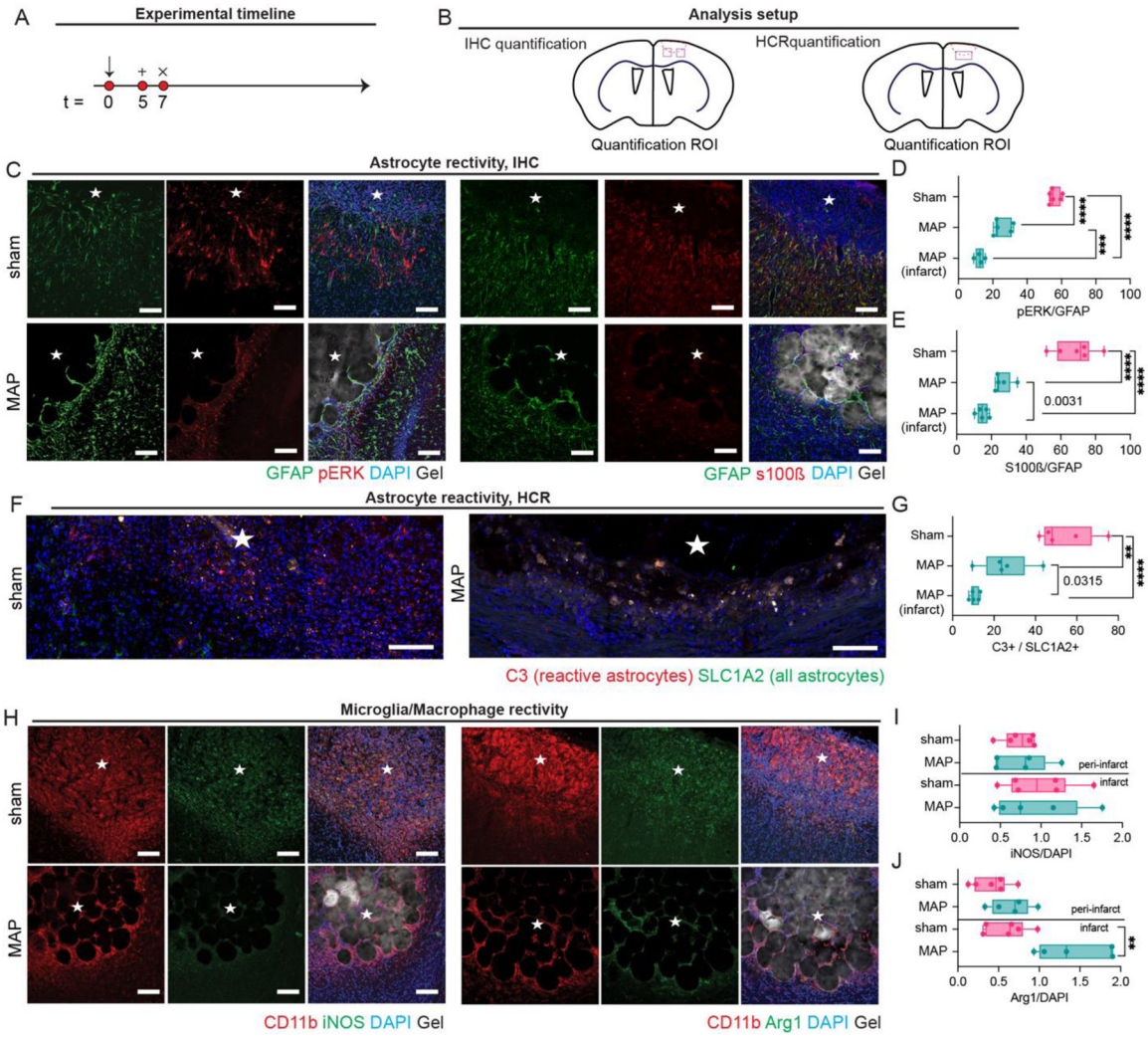

Figure 3.

A. Schematic of experimental timeline where arrow signifies stroke day, + signifies injection day (MAP only), and x signifies sacrifice and analysis time point. Sham is stroke only with no injection. B. Schematic of analysis setup showing where sections were imaged and analyzed. C. IHC images showing astrocyte reactivity through pERK, S100β, GFAP. D. Quantification of pERK/GFAP percent of astrocytes that are highly reactive. E. Quantification of S100β/GFAP percent of astrocytes that are highly reactive. F. In situ hybridization images of astrocyte reactivity through C3 and SLC1A2 probing. G. Quantification of C3/SLC1A2 percent of astrocytes that are highly reactive. H. IHC images of microglia reactivity through CD11b, Arg1, and iNOS staining. I. Quantification of iNOS/DAPI for determination of microglial pro-inflammatory phenotype. J. Quantification of Arg1/DAPI for determination of microglial pro-repair phenotype. All scale bar = 100μm. All measurements were done on FIJI. Statistical analysis was done in GraphPad Prism using one-way ANOVA analysis of variance followed by a multiple comparisons test comparing each condition (Tukey). The dots in each plot indicate the number of animals (n = 5 biological replicates) that were analyzed per-group and were considered independent

experiments. *, **, ***, **** means $p < 0.05$, 0.01, 0.001, 0.0001. Individual p-values in G indicate t-test between the condition indicated. ☆ represents the stroke cavity.

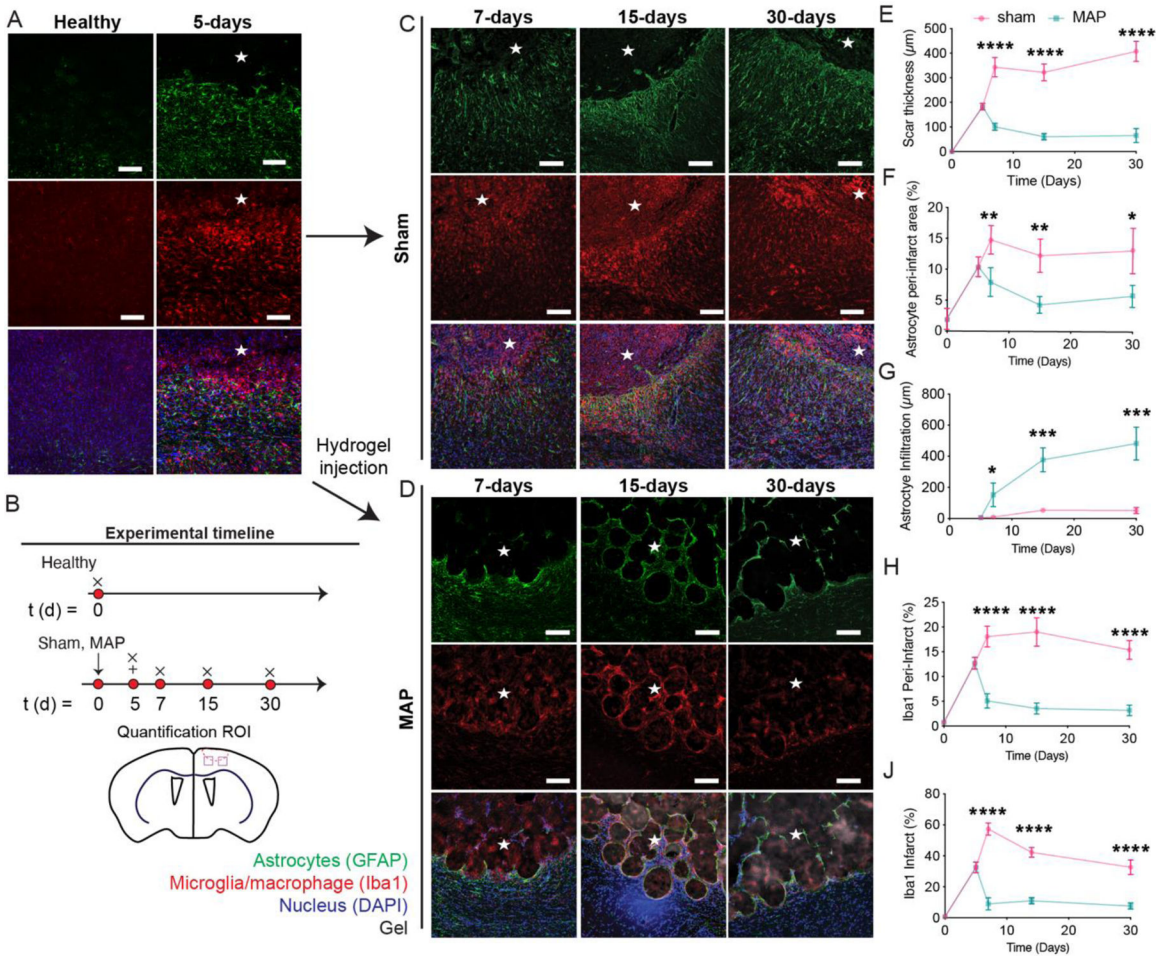

Figure 4.

A. IHC images showing reactive astrocytes and microglia of healthy tissue and 5 days post stroke. B. Schematic of experimental timeline where arrow signifies stroke day, + signifies injection day (MAP only), and x signifies sacrifice and analysis time point. Sham is stroke only with no injection. C. IHC images of sham stroke tissue showing reactive astrocytes and reactive microglia at 1-, 2-, 4-weeks post stroke through GFAP and Iba1 staining. D. IHC images of MAP gel treated stroke tissue showing reactive astrocytes and reactive microglia at 1-, 2-, 4-weeks post stroke through GFAP and Iba-1 staining. E. Quantification of scar thickness over time through GFAP staining comparing sham and HA-MAP treated brains. F. Quantification of percent area of reactive astrocytes in the peri-infarct through GFAP staining comparing sham and HA-MAP treated brains. G. Quantification of astrocyte infiltration into infarct through GFAP staining comparing sham and HA-MAP treated brains. H. Quantification of percent area of reactive microglia in peri-infarct area through Iba-1 staining comparing sham and HA-MAP treated brains. I. Quantification of percent area of reactive microglia in infarct through Iba-1 staining comparing sham and HA-MAP treated brains. All scale bars = 100μm. All measurements were done on FIJI. Statistical analysis was done in GraphPad Prism using two-way ANOVA analysis of variance followed by a multiple comparisons test (Sidak) comparing between condition at each timepoint. The dots in each plot indicate the number of animals (n = 5 biological replicates) that were analyzed

per-group and were considered independent experiments. *, **, ***, **** means $p < 0.05$, 0.01, 0.001, 0.0001. ✯ represents the stroke cavity.

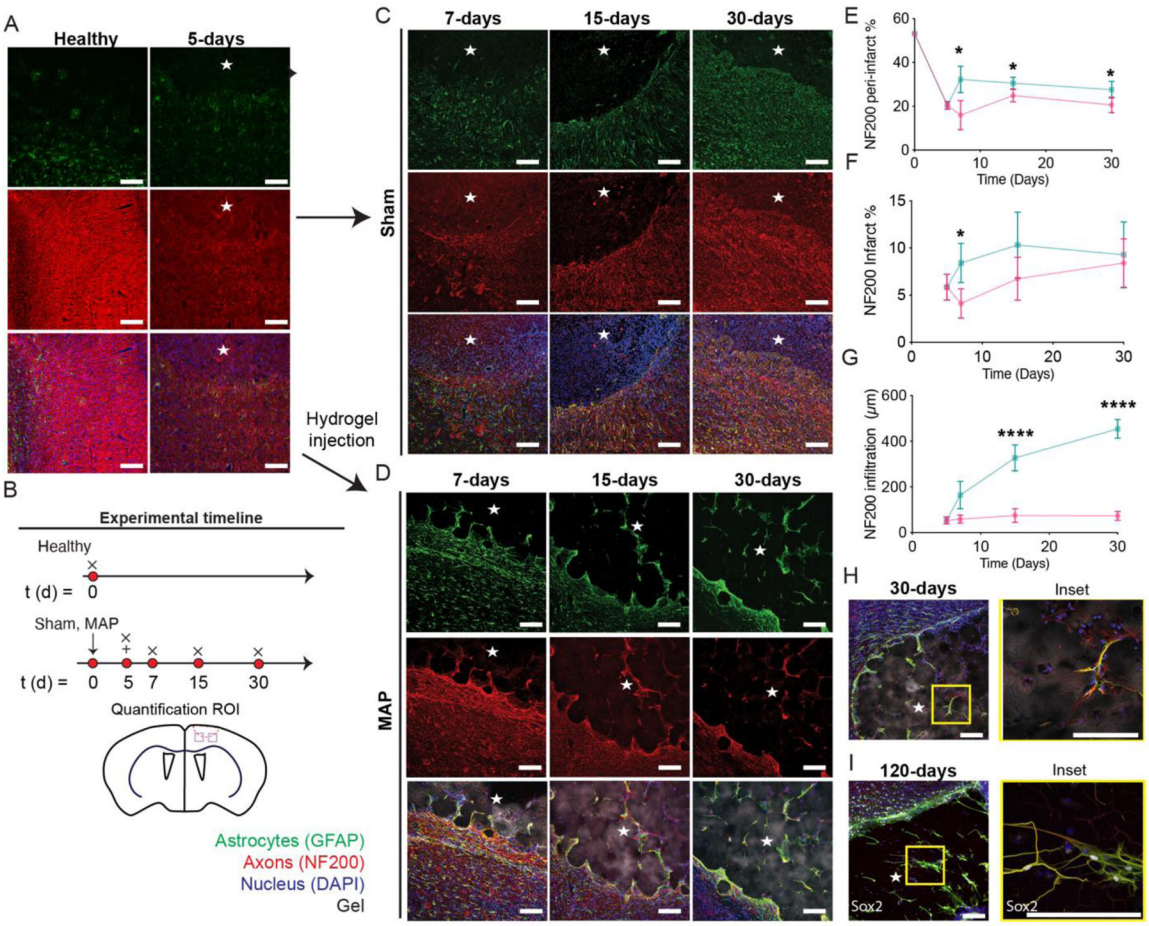

Figure 5.

A. IHC images showing reactive astrocytes and axons of healthy tissue and 5 days post stroke through GFAP and NF200 staining. B. Schematic of experimental timeline where arrow signifies stroke day, + signifies injection day (MAP only), and x signifies sacrifice and analysis time point. Sham is stroke only with no injection. C. IHC images of sham stroke tissue showing reactive astrocytes and axons at 1-, 2-, 4-weeks post stroke through GFAP and NF200 staining. D. IHC images of MAP gel treated stroke tissue showing reactive astrocytes and axons at 1-, 2-, 4-weeks post stroke through GFAP and NF200 staining. E. Quantification of percent area of axons in the peri-infarct through NF200 staining comparing sham and HA MAP treated conditions. F. Quantification of percent area of axons in the infarct through NF200 staining comparing sham and HA MAP treated conditions. G. Quantification of axon infiltration distance into infarct through NF200 staining comparing sham and HA MAP treated conditions. H. IHC images of co-residing astrocytes and axons at 4-weeks post stroke through GFAP and NF200. I. IHC images of co-residing astrocytes and axons at 120 days post stroke through GFAP and NF200. All scale bars = 100μm. All measurements were done on FIJI. Statistical analysis was done in GraphPad Prism using two-way ANOVA analysis of variance followed by a multiple comparisons test (Sidak) comparing between condition at each timepoint. The dots in each plot indicate the number of animals (n = 5 biological replicates) that were analyzed per-group and were considered

independent experiments. *, **, ***, **** means $p < 0.05$, 0.01, 0.001, 0.0001. ✯ represents the stroke cavity.

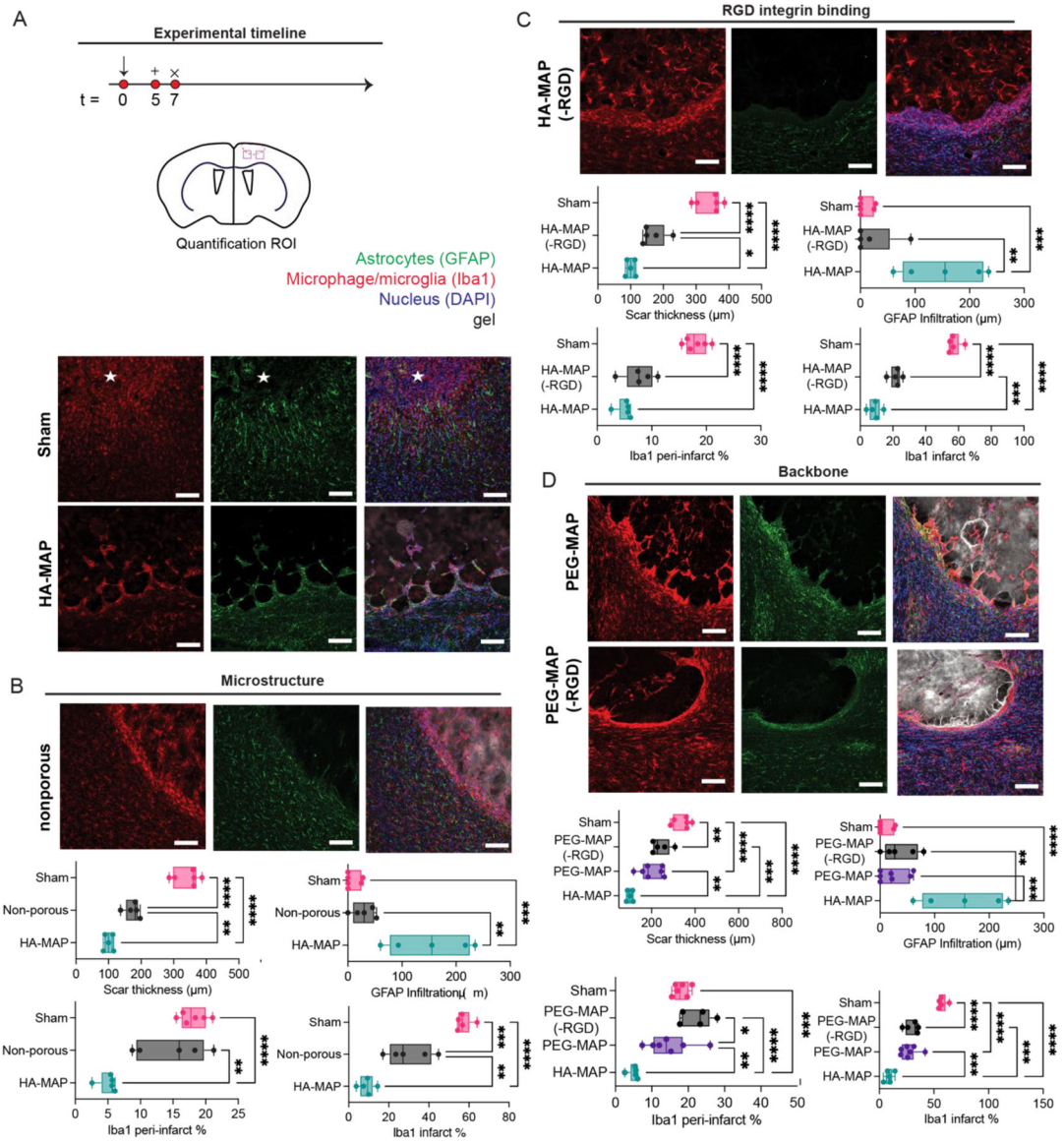

Figure 6.

A. Schematic of experimental timeline where arrow indicates day of stroke, + indicates day of injections, and x indicates day of sacrifice and analysis. IHC images for sham and HA MAP treated brains at 1 week post stroke staining for GFAP and Iba1. B. IHC images of non-porous treated brains staining for GFAP and Iba1. Quantification of reactive astrocytes and reactive microglia testing for scar thickness, astrocyte infiltration distance, Iba1 peri-infarct percent area, and Iba1 infarct percent area to analyze the role of hydrogel microstructure through GFAP and Iba1 staining. C. IHC images of HA MAP (-RGD) treated brains staining for GFAP and Iba1. Quantification of reactive astrocytes and reactive microglia testing for scar thickness, astrocyte infiltration distance, Iba1 peri-infarct percent area, and Iba1 infarct percent area to analyze the role of RGD integrin binding through GFAP and Iba1 staining. D. IHC images of PEG-MAP and PEG-MAP (-RGD) treated brains staining for GFAP and Iba1. Quantification of reactive astrocytes and reactive

microglia testing for scar thickness, astrocyte infiltration distance, Iba1 peri-infarct percent area, and Iba1 infarct percent area to analyze the role of hydrogel backbone through GFAP and Iba1 staining. All scale bars = 100μm. All measurements were done on FIJI. Statistical analysis was done in GraphPad Prism using one-way ANOVA analysis of variance followed by a multiple comparisons test comparing each condition (Tukey). The dots in each plot indicate the number of animals (n = 5 biological replicates) that were analyzed per-group and were considered independent experiments. *, **, ***, **** means $p < 0.05$, 0.01, 0.001, 0.0001. ☆ represents the stroke cavity.